Ozbakkaloglu, Togay

Concrete-filled FRP tubes: Manufacture and testing of new forms designed for improved performance

Journal of Composites for Construction, 2013; 17(2):280-291

CONCRETE-FILLED FRP TUBES: MANUFACTURE AND TESTING OF NEW FORMS DESIGNED FOR IMPROVED PERFORMANCE

Togay OZBAKKALOGLU*

ABSTRACT

This paper reports on the development and testing of three new concrete-filled fiber reinforced polymer (FRP) tube (CFFT) systems. These CFFT systems were designed to enhance the effectiveness of square and rectangular FRP tubes in confining concrete. In the design of the rectangular CFFTs two different enhancement techniques were considered, namely corner strengthening and provision of an internal FRP panel. The technique used in the development of the square CFFT system involved the incorporation of four internal concrete-filled FRP cylinders as an integral part of the CFFT. The performance of these systems was investigated experimentally through axial compression tests of ten unique CFFTs. The results of the experimental study indicate that the new CFFT systems presented in this paper offer significantly improved performance over conventional CFFTs with similar material and geometric properties. Examination of the test results have led to a number of significant conclusions in regards to confinement effectiveness of each new CFFT system. These results are presented and a discussion is provided on the parameters that influenced the compressive behavior of these CFFT systems.

KEYWORDS: Fiber reinforced polymers; Concrete; Confinement; Columns; Tubes; Stress-strain behavior.

* Senior Lecturer, School of Civil, Environmental and Engineering, University of Adelaide, Australia. Tel : + 618 8303 6477; Fax : +618 8303 4359; Email: togay.ozbakkaloglu@adelaide.edu.au

INTRODUCTION

Upon the introduction of fiber-reinforced polymer (FRP) composites to the construction industry, the use of externally bonded FRP for strengthening reinforced concrete members has received much attention. As an important application of FRP composites, confinement of existing reinforced concrete columns with FRP jackets have been investigated extensively (e.g, Rochette and Labossiere 2000; Chaallal et al. 2003; Lam and Teng 2004; Hadi 2006; Ilki et al. 2008; Ozcan et al. 2010; Wu and Wei 2010; Ozbakkaloglu and Akin 2011; Wang et al. 2012). More recently, attention has turned to the potential applications of FRP composites for new structures. One such application, which has received much recent attention, involves the use of concrete-filled FRP tubes (CFFTs) as high-performance composite columns in earthquake-resistant construction of new structures (e.g. Mirmiran et al. 1998; Seible et al. 1999; Fam and Rizkalla 2001, 2002; Mirmiran et al. 2001; Fam et al. 2005; Shao and Mirmiran 2005; Ozbakkaloglu and Saatcioglu 2006, 2007; Ozbakkaloglu and Oehlers 2008a, 2008b; Mohamed and Masmoudi 2010; Zaghi et al. 2012; Ozbakkaloglu 2012). Existing studies have demonstrated the ability of CFFTs to develop very high inelastic deformation capacities under simulated seismic loading, which makes them an attractive alternative for construction of new earthquake-resistant columns (Yamakawa et al. 2003; Shao and Mirmiran 2005; Ozbakkaloglu and Saatcioglu 2006, 2007; Saatcioglu et al. 2008).

It is well understood that lateral confinement can enhance both the strength and ductility of concrete. CFFTs owe their improved deformation capacities to the confinement action provided by the surrounding FRP tube. In a circular CFFT that is subjected to concentric compression concrete is confined uniformly by the FRP tube. Unlike in circular CFFTs, however, concrete in square and rectangular CFFTs is not subjected to a uniform confining pressure, as the pressure provided by the tube varies over the cross-section. The confinement effectiveness of FRP tubes improves with the uniformity of confining pressure, and for this reason square and rectangular tubes provide less effective confinement than circular tubes. As a result, for similar levels of performance, square and rectangular CFFTs require more confinement, and hence more fibers in their tubes, than circular CFFTs. This could lead to significantly increased construction costs, which is concerning as square and rectangular columns are extensively used in reinforced concrete structures. Early research by Ozbakkaloglu and Saatcioglu (2007) and Ozbakkaloglu and Oehlers (2008b) have shown that the confinement effectiveness of square and rectangular tubes can be improved through alternative tube arrangements. It was experimentally demonstrated that through the provision of internal FRP ties or panels the confinement effectiveness of FRP tubes could be improved for both square and rectangular CFFTs. Further research is needed, however, to fully investigate the influence of various tube arrangements on the confinement effectiveness of square and rectangular CFFTs.

In the study presented in this paper, three unique CFFT systems were designed, manufactured and tested under axial compression. Two of these systems were used in the manufacture of rectangular CFFTs and the third system was used to manufacture a square CFFT. In the first rectangular CFFT system the technique of corners strengthening was employed. In the second system, the FRP tube system that was developed by Ozbakkaloglu and Oehlers (2008b), which comprised of an FRP tube with an integrated internal panel, was further developed through the investigation of various internal panel configurations. Finally, a new square CFFT system that incorporates internal concrete-filled FRP cylinders was developed. This paper first presents the design and manufacture of the all three CFFT systems. The results of the axial compression tests on these CFFTs are then presented, followed by a discussion on the influence of the important design parameters on the confinement effectiveness and resulting compressive behavior of the new square and rectangular CFFT systems.

EXPERIMENTAL PROGRAM

Test Specimens

The experimental program was set up to investigate the efficacy of the new FRP tube systems to improve the confinement effectiveness of rectangular and square CFFTs. A total of nine rectangular and a square CFFTs were manufactured and tested under axial compression. The specimens were 600 mm in height and had a 150x300 mm rectangular or a 200x200 mm square cross-section, measured at the concrete core. The rectangular specimens had a corner radius of 40 mm and the square specimen had a slightly more rounded corners with a 50 mm radius. Out of the nine rectangular specimens, one was designed as the reference specimen with no strengthening, 3 specimens were designed to study the influence of various levels of corner strengthening, and the remaining 5 to study the influence of the use of internal panels with different stiffness and connection details. Details of the test specimens are shown in Table 1. The specimens in Table 1 were labeled as follows: letters R and S were used in labeling rectangular and square specimens, respectively. The letter L and the number that followed it provided the number of FRP layers used on the external tube of the specimen. For the rectangular specimens, additional abbreviations of 'CS', 'IP', and 'RIP' were used to indicate 'corner strengthening', 'internal panel' and 'internal panel with a rounded connection' and they were followed by a number letter combination that, respectively, provided information about the number of additional FRP layers and their type (i.e. carbon FRP (CFRP) or glass FRP (GFRP)) used in the applied strengthening method.

Design of Test Specimens

The amount of confinement and corner radius of the rectangular specimens were established such that the stress strain relationship of the reference specimen RL3 would exhibit an almost flat second branch, without any significant strength softening or hardening, to form a reasonable baseline performance. Based on the results of the previous study by Ozbakkaloglu and Oehlers (2008a) it was decided that a tube with 3 layers of CFRP and 40 mm corner radius would lead to a stress-strain curve with such characteristics when used to confine 25 MPa concrete. The designs of the remaining rectangular tubes extended from that of the reference specimen RL3 to enable the investigation of the performance of the two unique CFFT designs presented in this paper. The design of the square CFFT that incorporates 4 concrete-filled FRP cylinders was influenced by the idea of using internal panels with rounded connections. Cross-sections of the CFFTs are shown in Fig.1. Considerations that lie behind the design of the CFFT systems presented in this paper are discussed in the following sections.

Rectangular CFFTs with corner strengthening

It has been reported in a large number of studies that in square and rectangular FRP-confined concrete specimens FRP rupture often occurs at or near one of the corners of the specimen (e.g. Lam and Teng 2003; Ozbakkaloglu and Oehlers 2008a; Wang and Wu 2008). Although, it is now well understood that increasing the corner radius of the specimens leads to an increased confinement effectiveness, this does not shift the failure location from the corner to a region along the span. The main motivation behind the design of the specimens with additional corner reinforcement was the understanding that a given FRP tube with a prismatic cross-section would have unutilized capacity at the time of failure of FRP tube at or one of its corners due to stress concentrations. To utilize this capacity the corners of the FRP tube or jacket would require strengthening, and the optimum design of these confinement systems would require the establishment of the amount of additional reinforcement to be provided at the corners so that the failure of the regions of stress concentrations could be delayed to occur simultaneously with the more global failure of the rest of the tube. To establish the optimum corner strengthening amount for the reference specimen of the present study, three different strengthening ratios were considered; Specimens RL3CS1C, RL4CS2C and RL3SC2C had strengthening ratios of 1.33, 1.50 and 1.67, respectively. Through the inspection of the failure location of these specimens important insights have been gained on this special design parameter, which are discussed later in the paper.

Rectangular CFFTs with an internal panel

The idea of incorporating an internal panel in rectangular FRP tubes to improve the confinement effectiveness of these tubes was first discussed in Ozbakkaloglu and Oehlers (2008b). In this study it was shown that a significant improvement on confinement effectiveness could be attained through the use of an internal panel. Although the specimens investigated in Ozbakkaloglu and Oehlers (2008b) had the same dimensions to the rectangular specimens of the present study, they had a smaller radius of 20 mm. Therefore, it was of initial interest to find out how the incorporation of an internal panel, which provided a significant enhancement on the behavior of a CFFT of lower confinement effectiveness (i.e., 20 mm corners), would affect the behavior of the more effectively confined (i.e., 40 mm corners) reference specimen RL3 of the present study. To investigate this, Specimen RL3IP3C with a 3-layer CFRP internal panel was manufactured. In addition to the presence of the internal panel, its stiffness and connection details were also identified as important design parameters and were investigated through consideration of the following specimens: Specimen RL3IP6C, with a 6-layer CFRP internal panel, was considered to investigate the influence of increasing the stiffness of the internal panel; Specimens RL3IP6G and RL3IP6G, with 6- and 9-layer GFRP internal panels, were considered to investigate the influence of manufacturing the internal panel using a material with a higher rupture strain and influence of varying the stiffness of the panel made of this material; finally Specimen RL3RIP3C, with a 3-layer CFRP internal panel that was connected to the external tube with curved connections of 40-mm radius, was considered to investigate the influence of rounding the internal connection (very much like the corners of the external tube) to reduce the stress concentrations experienced at these connections.

Square CFFT made of concrete-filled FRP cylinders

A single square CFFT, Specimen SL5, was designed through further development of the design philosophy that was originally adopted for Specimen RL3RIP3C. Four internal concrete-filled FRP cylinders were incorporated in the manufacture of Specimen SL5, which functioned as an integral part of the specimen. The main motivation behind the design of Specimen SL5 was to design a square CFFT that would exhibit a performance level that is similar to a circular CFFT of similar material and geometric properties.

Materials

The specimens were prepared using a single concrete mix with a design target strength of 25 MPa at 28 days. The testing of the specimens started after the attainment of the 35-day strength and continued for approximately 2 weeks. Concrete cylinder tests have been conducted through the testing program to accurately record the variations in the strength of unconfined concrete during testing. The cylinder strength of unconfined concrete f'_c varied between 27.4 and 28.6 MPa during the time of testing, with an average test period cylinder strength f'_c of 28 MPa. In addition to the cylinders, three plain concrete rectangular specimens with the same nominal dimensions to the rectangular CFFTs were manufactured and tested during the testing program to establish the in-place strength of unconfined concrete f'_{co}. These tests indicated that f'_{co} ranged between 26 and 27.4 MPa with an average value of 26.7 MPa for the test period. This led to an f'_{co}/f'_c ratio of 0.95, which is consistent with previously reported ratios for specimens of similar dimensions in Ozbakkaloglu and Oehlers (2008a) and with the factor of 0.9 recommended by Ozbakkaloglu and Saatcioglu (2004) for converting the cylinder strength to the compressive strength of concrete in structural members. The axial strain ε_{co} corresponding to this strength f'_{co} was established as 0.22% from the same test.

The external tubes of all the specimens were manufactured using unidirectional carbon fiber sheets. Two of the specimens that were designed with an internal panel had internal panels that were made of glass fibers. The properties of the carbon and glass fiber sheets used in the fabrication of the FRP tubes are given in Table 2. The table also reports the properties of FRP composites that were established through flat coupon tests conducted in accordance with ASTM D3039 (2008). The FRP properties shown in Table 3 are based on nominal fiber thicknesses and they were averaged from 5 nominally identical coupon specimens.

Manufacturing of Test Specimens

The FRP tubes were manufactured using a manual wet lay-up process by wrapping epoxy resin impregnated fiber sheets around precision-cut high-density Styrofoam moulds in the hoop direction. The external tubes of all the specimens were manufactured using unidirectional carbon fiber sheets which were wrapped around the templates one layer at a time. An overlap length of 100 mm was provided in all the external tubes to prevent premature debonding failure. The FRP tubes are shown in Fig.2. The manufacturing procedures used for each of the special forms are summarized in the proceeding sections.

Rectangular CFFTs with corner strengthening

The CFFTs with corner strengthening were manufactured by applying additional CFRP strips, with fibers oriented in the hoop direction, at the corners of the FRP tube along the entire height of the specimen. After wrapping the first layer of the CFRP sheet around the Styrofoam mould, an additional CFRP strip was applied at each corner of the tube. To ensure proper development of stresses, the strips were extended on each side of the corner by 25 mm beyond the curved region and were sandwiched between the first and second full layers of the tube. A final full layer of CFRP was then applied to complete the fabrication of the Specimen RL3CS1C with a 3-layer CFRP tube and a single layer of corner strengthening strips. To attain the desired corner strengthening ratios, the above process was repeated for Specimens RL3CS2C and RL4CS2C which respectively had 3- and 4-layer FRP tubes and additional corner strengthening strips made of 2 layers of CFRP.

Rectangular CFFTs with an internal panel

Two Styrofoam moulds with 150 mm square cross-sections were used to manufacture the CFFTs with internal panels. When joined together, the square tubes manufactured using these moulds formed a complete rectangular tube with an internal panel. All the internal panel specimens, except for the rounded internal panel specimen RL3RIP3C, were manufactured using square templates with 2 sharp (90 degree) corners and 2 rounded (40mm-radius) corners. These two tubes were joined together in a way to form a rectangular tube with rounded corners of 40 mm radius and 90 degree internal panel-external tube connection. Specimen RL3RIP3C was manufactured using square moulds with 40 mm corner radius on all four corners, which resulted in a final rectangular tube with a curved internal panel-external tube connection.

Once the square specimens were fabricated, they were left to dry. To attain the desired stiffness of the internal panel, additional layers of FRP were then applied on the faces of the square tubes that would form the internal panel of the rectangular tube when joined together. Once dry, the two square tubes were bonded together using of the same epoxy resin used in the impregnation of the fibre sheets. Finally, a full external layer of FRP was applied to cover the entire tube. All of the internal panel specimens had 3 layers of CFRP on their external tubes and their internal panels were made of either CFRP or GFRP with varying number of layers. Slightly different manufacturing methods had to be employed to fabricate the tubes with CFRP and GFRP internal panels, which resulted in slightly different fiber sheet lengths for Specimens RL3IP6C and RL3IP6G, as shown in Table1.

Square CFFT made of concrete-filled FRP cylinders

The manufacture of the square CFFT initially involved fabrication of four CFRP cylinders with 100 mm diameters. Each CFRP cylinder was manufactured with a single layer of CFRP which was provided with an overlap that covered the three quarters of the entire circumference. Once dry, the four cylinders were assembled together and served as the template for the manufacture of the external tube of the square CFFT. In assembling the cylinders, each cylinder was oriented in a way that the quarter of its circumference which had only one layer of CFRP would correspond to a corner of the finished square tube. Four layers of CFRP were then applied to the joined circular sections to form the external tube. Each of these layers had a 100 mm overlap, which was provided at a different tube face in each layer. The process summarized above resulted in a square external tube with five CFRP layers all around.

Instrumentation and testing

The specimens were instrumented with linear variable displacement transducers (LVDTs) and strain gauges to measure axial deformations as well as axial and transverse strains. Axial deformations of the columns were measured with a total of eight LVDTs, which were mounted at two different gauge lengths. Four of the LVDTs, mounted one on each face, covered a height of 200 mm at the mid-height region. Another four LVDTs were mounted at the corners between the loading and supporting steel plates of the test machine to measure average axial strains along the height of the specimens. In addition, axial strains at the mid-height were measured using four unidirectional strain gauges with a gauge length of 20 mm that were installed at the mid-span of each face of the specimens. Transverse strains of the rectangular CFFTs were measured by eight unidirectional strain gauges that were bonded on the FRP tube. Four of these strain gauges were installed at the mid-width of each face and the other four were placed at or near each corner as shown in Fig. 3. Transverse strains of the square CFFT was measured by six strain gauges, four of which were installed at the mid-width of each face and the other two placed at the corners as illustrated in Fig. 3.

The specimens were tested under axial compression using a 5000 kN capacity universal testing machine. During the initial elastic stage of the behavior, the loading was applied with load control at 3 kN per second, whereas displacement control was used at approximately 0.006 mm per second beyond the initial softening until specimen failure. Prior to testing, all specimens were capped at both ends to ensure uniform distribution of the applied pressure. In the tests of the rectangular CFFTs, the load was applied directly to the concrete core through precision-cut steel plates with dimensions that were 2 mm smaller than the cross-sectional dimensions of the CFFTs. The load was applied to the entire cross-section of the square CFFT, Specimen SL5. The test setup and instrumentation are shown in Fig.4.

TEST RESULTS AND DISCUSSION

Specimen failure modes

A number of different failure modes were observed in the CFFTs investigated in the present study. These are summarized in Table 3 for each specimen and the photographs of the specimens at the end of testing are shown in Fig. 5. A discussion on these failure models and related observations are presented next for each of the unique CFFT systems.

Reference CFFT

As shown in Fig. 5(a) the FRP tube of Specimen RL3 failed near one of its corners. This was expected and, as has been discussed previously (e.g. Lam and Teng 2003; Ozbakkaloglu and Oehlers 2008a; Wang and Wu 2008) is caused by the stress concentrations that occur at the section where the curved segment that forms the corner of the tube connects to the flat edge of the tube.

Rectangular CFFTs with corner strengthening

Similar to that observed for the reference specimen RL3, the tube of Specimen RL3CS1 failed near one of its corners (Fig.5(b)), indicating that the extra single layer provided at the corners of the tube was not enough to shift the failure location away from the corners. On the other hand, as illustrated in Figs. 5(c) and 5(d), for both Specimens RL3CS2 and RL4CS2 with two additional corner layers the failure occurred away from the corners. These observation indicate that for the rectangular CFFTs of the present study the minimum amount of additional corner strengthening that would be required to shift the failure location away from the corners of the tube was somewhere between 33 and 50% of the original thickness of the FRP tube. This is discussed further later in the paper.

Rectangular CFFTs with an internal panel

As summarized in Table 3 the failures of the specimens with internal panels occurred at a number of different regions. Specimen RL3IP3C experienced a partial failure of its internal panel which was accompanied by the rupture of the external tube near the internal panel connection (Fig. 5(e)). The failure of Specimen RL3RIP3C with a rounded internal panel connection occurred at the internal panel where the panel ruptured near the connection of its curved and flat segments, as shown in Fig. 5(f). The failure locations of the remaining specimens with internal panels, however, were isolated to the external tube and the internal panel remained intact without any signs of damage. Both Specimens RL3IP6C and RL3IP6G, with panels made of 6 layers of CFRP and GFRP respectively, failed as result of the rupture of the external tube near the internal panel connection (Figs. 5(g) and 5(h)). Specimen RL3IP9G with 9 layers of GFRP failed near one of the corners of its external tube as illustrated in Fig. 5(i).

Square CFFT made of concrete-filled FRP cylinders

The square specimen SL5 failed as a result of the rupture of the external tube near one of its corners as shown in Fig. 5(j). Dissection of the specimen revealed that the internal circular tubes also experienced significant damage especially along the regions of the tubes that corresponded to the corners of the external tube (Fig. 5(j)).

Transverse strains at failure

The recorded transverse strains at failure are shown in Table 4 for each specimen. For the rectangular CFFTs, the average strains calculated from eight strain gauges are reported together with the strains recorded at short-span, long-span, corner and near corner regions (each averaged from two strain gauges). For the square CFFT, the average strain from six strain gauges, span strains averaged from four strain gauges and corner strains averaged from two strain gauges are provided.

The results reported in Table 4 illustrates that all of the corner strengthened specimens were able to develop larger short-span and long-span strains compared to the control specimen RL3. This indicates that strengthening of tube corners allow the development of larger confinement pressures by delaying the failure of the tube at locations of stress concentrations near the corners. In Table 4, comparison of the long- and short-span strains of the specimens having an internal panel with those manufactured without one points to an important influence of the internal panel on the distribution of transverse strains on external FRP tube. That is, the specimens having an internal panel consistently developed larger long-span strains than short-span strains, as opposed to the specimens without an internal panel, which, as expected, developed larger strains along their short-spans. Another interesting observation from the transverse strains reported in Table 4 is that the square CFFT SL5 demonstrated a highly uniform transverse strain distribution, developing almost identical average strains at the corners and along the spans. As discussed previously, the confinement effectiveness of FRP tubes increases with the uniformity of confining pressure, hence the above observation points to the high confinement effectiveness of the square CFFT. This is supported by the observations from the axial stress-strain behavior of the specimen, as discussed in detail in the following section.

Axial stress-strain behavior

The summary of the key experimental results are shown in Table 5, which includes: the ultimate axial strength and strain of the specimens (f'_{cc} *and* ε_{cu}), the axial stress that corresponds to the point of transition from the initial ascending branch to the second branch of the stress-strain curve (f'_{ct}), and the strength and strain enhancement ratios (f'_{cc}/f'_{co} *and* $\varepsilon_{cu}/\varepsilon_{co}$). Additionally, ultimate strength to transition stress ratios (f'_{cc}/f'_{ct}), which provide useful information about the overall trends of the second branches of the stress-strain curves, are also shown in Table 5. The ultimate confined-concrete strengths f'_{cc} reported in the table were calculated from the recorded axial loads just prior to the failure of the specimens. The ultimate axial strain of confined concrete ε_{cu} was averaged from the four corner LVDTs. A closer inspection of the results reported in Table 5 reveals that transition stresses f'_{ct} of some of the specimens were slightly lower than the in-place strengths of the unconfined concrete f'_{co} established from the tests of plain control specimens as discussed previously. This suggests that for the CFFTs of the present study the strength of the unconfined concrete inside the FRP tubes was slightly lower than the strength obtained for the same concrete from the tests of a prism with the same dimensions. This slight disparity was probably caused by the differences in the formworks used for the CFFTs and plain concrete specimens (i.e. FRP stay-in-place formwork versus sacrificial timber formwork) and the resulting differences in the curing conditions of the specimens. Figures 6 to 11 show the axial stress-strain curves of the test specimens. Based on the results presented in these figures and reported in Table 5, the following section provides a discussion on the influence of the important design parameters on the compressive behavior of the each new CFFT system presented in this paper. As noted in Table 5, Specimen RL3IP9G failed prematurely as a result of load eccentricity experienced during the test that was caused by manufacture imperfections, and hence the specimen was excluded from the following discussion.

Rectangular CFFTs with corner strengthening

Figure 6 illustrates the influence of corner strengthening on the axial stress-strain behavior of the rectangular CFFTs. The comparison of the stress-strain curves of Specimens RL3 and RL3CS1C indicates that the ultimate axial strain of CFFTs can be increased significantly through corner strengthening. As can be seen from the $\varepsilon_{cu}/\varepsilon_{co}$ ratios given in Table 5, this increase was around 40% for Specimen RL3CS1C over the reference specimen RL3. The addition of the second corner layers resulted in a further increase in the ultimate strain, which is evident from the comparison of the curves of Specimens RL3CS1C and RL3CS2C in Fig.6. However, the additional increase was only around 10%, indicating that the second corner layer did not provide as much enhancement as the first one. Examination of the failure modes of Specimens RL3CS1C and RL3CS2C provides further insight into the differences in the relative effectiveness of the first and second layer of corner FRP strips. As discussed previously Specimen RL3CS1C failed near one of its corners, whereas the failure of the Specimen RL3CS2C occurred at a region along one of the long-spans of the tube. This shift in the failure location indicates that the additional corner reinforcement provided in Specimen RL3CS2C overstrengthened its corners with respect to the rest of the tube. This also implies that the second layer of corner reinforcement was not fully utilized. As discussed previously the failure location of Specimen RL4CS2C was similar to that of Specimen RL3CS2C, which indicates that for the rectangular CFFTs of the present study increasing the FRP thickness of the corner regions by 50% or more over the original thickness of the tube resulted in overstrengthening of the corners. These observations suggest that an optimal level of corner strengthening, which can be defined as the minimum amount of additional corner strengthening required to shift the failure location away from the corners of the tube, can be established for CFFTs as a function of their geometric properties. It would be reasonable to assume that both the corner radius and sectional aspect ratio would influence this optimal strengthening ratio. For example, specimens with smaller corners would likely benefit from higher strengthening ratios due to higher stress concentrations they experience near their corners.

Figure 6 also illustrates that the overall trend of the second branches of the stress-strain curves of the CFFTs were also influenced to some extent by the presence of the additional corner layers, which resulted in increased f'_{cc}/f'_{ct} ratios for the corner strengthened specimens over the reference specimen RL3, as can be seen in Table 5. This implied increase in the confinement effectiveness can be explained by the additional diagonal confining forces resulted from the presence of the additional corner layers.

To further illustrate the influence of corner strengthening, in Fig.7 the stress-strain curve of Specimen RL4CS2C with a 4-layer tube strengthened by 2 layers of corner strips is shown together with the curve of a CFFT (R1R40L5) previously reported in Ozbakkaloglu and Oehlers (2008a). The FRP tube of Specimen R1R40L5 was made of the same carbon fibers used in the CFFTs of the present study and it consisted of 5 full layers of CFRP. The unconfined concrete strength of Specimen R1R40L5 was around 3 MPa lower than that of Specimen RL4CS2C and the specimens had the same dimensions. Stress-strain curves of the specimens shown in Fig.7 illustrates that the axial compressive behaviors of these specimens were almost identical, with Specimen R1R40L5 developing a slightly higher ultimate axial strain and Specimen RL4CS2C exhibiting a higher second branch slope. This observation indicates that the additional confinement provided by the corner layers was sufficient to compensate for the reduced FRP thickness of the tube. This observation also points to the possibility of reducing the amount of FRP used in CFFTs without compromising their performance through more efficient placement of fibers around the perimeter of the tubes. Such design arrangements could lead to significant savings especially in larger members.

Rectangular CFFTs with an internal panel

Figure 8 shows the influence of the presence and properties of an internal panel on the axial stress-strain behavior of the rectangular CFFTs. The comparison of the stress-strain curves of the specimens having an internal panel with the curve of the reference specimen RL3 demonstrates that incorporation of an internal panel leads to a significant improvement on both the ultimate strength f'_{cc} and axial strain ε_{cu} of rectangular CFTTs. As evident from Fig.8, the overall trends of the second branches of the stress-strain curves were significantly influenced by the presence of an internal panel. This is also reflected in the f'_{cc}/f'_{ct} ratios shown in Table 5. These observations indicate that the presence of an internal panel improves the compressive behavior of rectangular CFFTs both through increasing the confinement effectives and delaying the rupture of their tubes. A closer inspection of the curves shown in Fig.8 leads to a number of interesting observation in regards to the influence of the internal panel parameters on the compressive behavior this new CFFT system. Comparison of the curves of Specimens RL3IP3C and RL3IP6C reveals that the increased stiffness of the internal panel of the latter specimen resulted in a more steeply ascending second branch and a slightly increased ultimate axial strain ε_{cu}. This suggests that the confinement effectiveness of the tube increases with an increase in the stiffness of the internal panel. As discussed previously, at the end of testing there were signs of damage on the internal panel of the Specimen RL3IP3C with a 3-layer CFRP internal panel, which was not observed in the 6-layer CFRP panel of the Specimen RL3IP6C. On the other hand, fairly close ultimate axial strains of the two specimens suggests that the panel damage was not a main contributor to the eventual failure of Specimen RL3IP3C.

The 6-layer GFRP internal panel of Specimen RL3IP6G was designed to exert a similar axial force to the 6-layer CFRP panel of Specimen RL3IP6C. The panel of Specimen RL3IP6G, however, had a lower axial stiffness and a higher axial elongation capacity than the panel of Specimen RL3IP6C. Comparison of the stress-strain curves of the two specimens in Fig.8 illustrates the influence of the axial stiffness and elongation capacity of the internal panel on the compressive behavior of these CFFTs. The figure shows that the slope of the second branch of Specimen RL3IP6C with higher panel stiffness was slightly higher than that of Specimen RL3IP6G. However, the ultimate strain ε_{cu} of Specimen RL3IP6G with an internal panel made of a material with a higher rupture strain was significantly higher than that observed in the companion specimen RL3IP6C. This comparison clearly illustrates that the substitution of GFRP panel in place of CFRP panel resulted in an overall improvement on the compressive behavior of the specimens. As mentioned previously Specimen RL3IP9G with a 9-layer GFRP internal panel failed prematurely, and hence it was excluded from the above comparison.

The comparison of the stress-strain curves of Specimens RL3RIP3C and RL3IP3C in Fig.8 illustrates the influence of the internal panel external tube connection detail. Specimen RL3RIP3C with a rounded connection exhibited a stress-strain curve with a much more steeply ascending second branch compared to that of Specimen RL3IP3C with a 90 degree connection. In fact, the second ascending branch of Specimen RL3RIP3C had the largest slope among all the rectangular CFFTs of the present study. This indicates that the confinement effectiveness of the tubes with internal panels can be further increased through the use of rounded panel-tube connections. However, as evident from Fig.8 and Table 5, a similar improvement was not observed in the ultimate axial strain ε_{cu}. As was discussed previously the failure of the Specimen RL3RIP3C was caused by the rupture of the internal panel, suggesting that an increased panel stiffness could potentially lead to an increased ultimate strain and further improvement on the behavior of this unique CFFT system.

To investigate the influence of the corner radius of the external tube on the behavior of CFFTs with an internal panel, the stress-strain curve of a CFFT (Specimen R20L3W) from Ozbakkaloglu and Oehlers (2008b) is shown in Fig.9 together with the curves of the two selected specimens of the present study. These specimens had almost the same unconfined concrete strength, and apart from its 20 mm tube corner radius, Specimen R20L3W was identical to Specimen RL3IP3C. Comparison of the stress-train curves of the aforementioned specimens in Fig.9 illustrates that corner radius influences the behavior of CFFTs with an internal panel in two ways. First, as has been reported previously (e.g. Lam and Teng 2003; Ozbakkaloglu and Oehlers 2008a; Wang and Wu 2008) an increase in corner radius leads to increased confinement effectiveness, which is reflected as increased slope of the second branch in stress-strain curves. In addition to this, the corner radius appears to also influence the ultimate axial strain of CFFTs. As evident from the comparison of the curves of Specimens RL3IP3C and R20L3W in Fig.9, increased corner radius results in a decrease in the ultimate axial strain of the CFFT. On the other hand, the stress-strain curve of Specimen RL3IP6G of the present study shown in the same figure illustrates that CFFTs with internal panels can be designed to attain higher ultimate strains without compromising their confinement effectiveness. Specimen RL3IP6G had the same ultimate strain as Specimen R20L3W, yet the stress-strain curve of the former specimen exhibited a much steeper ascending branch than the latter, as illustrated in Fig.9.

Relative performance of rectangular CFFTs

To investigate relative performances of the two unique rectangular CFFT systems presented in this study, stress-strain curves of the selected specimens are shown in Fig.10, with the strength and strain enhancement ratios of all the specimens given in Table 6. Table 6 also shows the total length of the FRP used in each specimen (S_{spec}) with respect to the total length of FRP used in the reference specimen RL3 (S_{ref}). As illustrated by S_{spec}/S_{ref} ratios in Table 6, the total FRP sheet lengths used in the fabrication of the specimens shown in Fig.10 were quite similar. From the stress-strain curves shown in Fig. 10 it is clear that corner strengthening is highly effective for increasing the ultimate strain of rectangular CFFTs, however it influences the trend of the second branch of the curve only marginally. Provision of an internal panel in rectangular CFFTs, on the other hand, leads to a significant increase in confinement effectives, which results in a much improved trend of the second branch of the stress-strain curve as evident in Fig.10. Therefore, if the main objective is to design a CFFT with higher confinement effectiveness, then of the two CFFT systems, the CFFTs with an internal panel would provide a more attractive alternative over the corner strengthened ones. On the other hand, in cases where confinement effectiveness of the confining tube is sufficiently high, as in square CFFTs with well-rounded corners that are made of normal-strength concrete, the corner strengthening method could be used satisfactorily to attain the desired ultimate axial strain capacity.

Square CFFT made of concrete-filled FRP cylinders

The stress-strain curve of the square specimen SL5 is shown in Fig.11. In this figure stress-strain curve of another square CFFT (Specimen SR40L5 from Ozbakkaloglu and Oehlers (2008b)) of the same external dimensions and unconfined concrete strength is also shown. Specimen SR40L5 consisted of a 5-layer CFRP tube that was manufactured using the same carbon fiber sheets used in the specimens of the present study and had a tube corner radius of 40mm. These similar material and geometric properties made Specimen SR40L5 and ideal comparison specimen to Specimen SL5. Figure 11 illustrates the remarkable difference in the confinement effectiveness of these two CFFT systems. As can be seen in the figure Specimens SL5 and SR40L5 developed almost the same ultimate axial strain. On the other hand, the second branch slope of Specimen SL5 was more than twice that of Specimen SR40L5. This observation points to the extremely high confinement effectiveness of the new CFFT system, especially when considered in light of the fact that the confinement effectiveness of Specimen SR40L5 was already high due to its large tube corner radius. To gain further insight into the relative performance level of Specimen SL5, the ultimate axial strength f'_{cc} and strain ε_{cu} of the specimen was to be compared with those from a circular CFFT with similar geometric and material properties. However, because a circular specimen with a fully compatible set of parameters was not available in the literature, the ultimate strength and strain of a companion circular CFFT was predicted using 5 different models of FRP-confined concrete (i.e., Berthet 2006; Teng et al. 2007, 2009; Youssef et al. 2007; Wei and Wu 2012) an these predictions were used in the comparison. The model predictions reported in Table 7 were based on a circular specimen with a 200 mm cross-section, 26.7 MPa unconfined concrete strength and a jacket made of 5 layers of the same CFRP sheets used in the present study. The model prediction to experimental result ratios for the ultimate strength $(f'_{cc})_{model}/(f'_{cc})_{SL5}$ and ultimate strain $(\varepsilon_{cu})_{model}/(\varepsilon_{cu})_{SL5}$ are also shown in Table 7. These results illustrate that the new square CFFT system presented in this paper offers performance levels that match or exceed those typically observed in circular CFFTs.

CONCLUSIONS

This paper has presented the details of three new CFFT systems, as well as the results of axial compression tests conducted on them. Based on the results and discussions presented in the paper the following conclusions can be drawn:

1. All three new CFFTs systems presented in this paper offer improved performance under axial compression compared to conventional CFFTs with similar material and geometric properties.
2. Through corner strengthening the ultimate axial strains of CFFTs can be increased significantly. This method also provides some improvement on the overall trend of the second branch of the stress-strain curve of CFFTs.
3. CFFTs with corner strengthening may exhibit similar levels of performance with CFFTs having thicker FRP tubes. This indicates that through more efficient placement of fibers around the cross-section of the tube, total fiber content of the tube can be reduced.
4. To optimize the design of CFFTs with corner strengthening it is important to establish the corner strengthening ratio at which the failure location shifts away from the corners of the tube to a region along its span. For the CFFTs of the present study, with a sectional aspect ratio of 2.0 and corner radius of 40 mm, this ratio was between 1.33 and 1.50. Further research is needed to understand the influence of the sectional aspect ratio and corner radius on the optimum strengthening ratio.
5. Provision of an internal FRP panel leads to a significant increase in the confinement effectiveness of rectangular FRP tubes, and CFFT systems manufactured using these tubes demonstrate substantially improved compressive behavior compared to conventional rectangular CFFTs.
6. The behavior of CFFTs with an internal panel is influenced significantly by the properties and the connection details of the internal FRP panel. Increasing the panel stiffness, changing the panel material to a material with a higher rupture strain (i.e. GFRP in place of CFRP) and using a rounded panel connection instead of a 90 degree one are all shown to have positive effects on the compressive behavior of this CFFT system.

7. Corner radius of the tube appears to influence the stress-strain behavior of CFFTs with an internal panel in much the same manner as it does conventional square and rectangular CFFTs. Further investigation is required, however, to better understand the combined influence of the internal panel parameters and corner radius on the confinement effectiveness of this new CFFT system.
8. The new square CFFT system presented in this paper offers an extremely high confinement effectiveness that rivals circular CFFTs. The axial compressive behavior of this new CFFT system has been shown to resemble that of a circular, rather than a square, CFFT.

ACKNOWLEDGEMENTS

The author would like to thank Ms. Sadri and Messrs. Haigh, Kohler and Richter, who have undertaken the tests reported in this paper as part of their undergraduate theses. This research is part of an ongoing programme at The University of Adelaide on FRP-concrete composite columns.

REFERENCES

ASTM D 3039/D 3039M-08 (2008). "Standard test method for tensile properties of polymer matrix composite materials. ASTM International." West Conshohocken, PA, p. 13.

Bisby, L.A., Dent, A. J. S., Green, M. F. (2005). “Comparison of confinement models for fiber-reinforced polymer-wrapped concrete.” ACI Struct. J., 2005. 102(1): p. 62-72.

Chaallal, O., Hassan, M., Shahawy, M. (2003). “Confinement model for axially loaded short rectangular columns strengthened with fiber reinforced polymer wrapping.” ACI Struct J 2003; 100(2): 215–21.

Fam, A. Z., and Rizkalla, S. H. (2001). “Behavior of Axially Loaded Concrete-Filled Circular Fiber-Reinforced Polymer Tubes.” ACI Structural Journal, 98, 3, pp 280-289.

Fam, A. Z., and Rizkalla, S. H. (2002). “Flexural behavior of concrete-filled fiber reinforced polymer circular tubes.” *Journal of Composites for Construction*, 6(2), 123-132.

Fam, A., Schnerch, D. and Rizkalla, S. (2005). "Rectangular Filament-Wound GFRP Tubes Filled with Concrete under Flexural and Axial Loading: Experimental Investigation." Journal of Composites for Construction, ASCE, Vol. 9, No. 1, pp 25-33.

Hadi, M. N. S. (2006) "Behaviour of FRP wrapped normal strength concrete columns under eccentric loading." J. Compos. Struct., 2006. **72**(4): p. 503-511.

Ilki A, Peker O, Karamuk E, Demir C, Kumbasar N. (2008). "FRP retrofit of low and medium strength circular and rectangular reinforced concrete columns." J. Mater Civ Eng, ASCE; 20(2): 169-88.

Lam, L., and Teng, J.G. (2003). "Design-oriented stress-strain model for FRP-confined concrete in rectangular columns." Journal of Reinforced Plastics and Composites, 22(13), 2003, pp 1149–1186.

Lam, L., and Teng, J. G. (2004). "Ultimate condition of fiber reinforced polymer-confined concrete." Journal of Composites for Construction, ASCE, 8(6), 539-548.

Mirmiran, A., Shahawy, M., and Beitleman, T. (2001). "Slenderness Limit for hybrid FRP-concrete columns." Journal of Composites for Construction, ASCE, 5, 1, pp 26-34.

Mirmiran, A., Shahawy, M., Samaan, M., El Echary, H., Mastrapa, J.C., and Pico, O. (1998). "Effect of Column Parameters on FRP-confined Concrete." Journal of Composites for Construction, ASCE, 2, 4, pp 175-185.

Mohamed, H., and Masmoudi, R. (2010). "Axial Load Capacity of Concrete-Filled FRP Tube Columns: Experimental versus Predictions." J. Compos. Constr., ASCE, 14(2): p. 231-243.

Ozbakkaloglu, T. (2012) "Axial Compressive Behavior of Square and Rectangular High-Strength Concrete-Filled FRP Tubes." Journal of Composites for Construction, ASCE. DOI: 10.1061/(ASCE)CC.1943-5614.0000321

Ozbakkaloglu, T., and Akin, E. (2012). "Behavior of FRP-confined normal- and high-strength concrete under cyclic axial compression." Journal of Composites for Construction, ASCE, 16(4), 451-463.

Ozbakkaloglu, T., and Oehlers, D. J. (2008a). "Concrete-filled Square and Rectangular FRP Tubes under Axial Compression." Journal of Composites for Construction, ASCE, Vol.12, No.4, pp.469-477.

Ozbakkaloglu, T. and Oehlers, D. J. (2008b). "Manufacture and testing of a novel FRP tube confinement system." Engineering Structures, 30, 2448-2459.

Ozbakkaloglu, T., and Saatcioglu., M. (2004). "Rectangular Stress Block for High-Strength Concrete." ACI Structural Journal, V. 101, No. 4, pp. 475-483.

Ozbakkaloglu, T., and Saatcioglu, M. (2006). "Seismic behavior of high-strength concrete Columns confined by fiber reinforced polymer tubes." Journal of Composites for Construction, ASCE, 10(6), 538-549.

Ozbakkaloglu, T., and Saatcioglu, M. (2007). "Seismic performance of square high-strength concrete columns in FRP stay-in-place formwork." Journal of Structural Engineering, ASCE, 133(1), 44-56.

Ozcan, O., Binici, B., Ozcebe, G. (2010). "Seismic strengthening of rectangular reinforced concrete columns using fiber reinforced polymers." Eng Struct; 32(4): 964–73.

Rochette, P., and Labossiere, P. (2000). "Axial Testing of Rectangular Column Models Confined with Composites." Journal of Composites for Construction, ASCE, 4, 3, pp 129-136.

Saatcioglu, M., Ozbakkaloglu, T., Elnabelsy, G. (2008) "Seismic behavior and design of reinforced concrete columns confined with FRP stay-in-place formwork." ACI SP-257, p. 145-165.

Seible F, Karbhari VM, Burgueno R. (1999). "Kings stormwater channel and I-5/Gilman bridges, USA." Journal of the International Association for Bridge and Structural Engineering (IABSE), Structural Engineering International; 9(4):250–3.

Shao, Y., and Mirmiran, A. (2005). "Experimental Investigation of Cyclic Behavior of Concrete-Filled FRP Tubes," Journal of Composites for Construction, ASCE, 9(3), 263-273.

Teng, J.G., Huang, Y. L., Lam, L., and Ye, L. (2007). "Theoretical model for fiber reinforced polymer confined concrete." ASCE J. Compos. Constr. 11(2): p. 201-210.

Teng, J.G., Jiang, T., Lam, L. and Luo, Y. (2009). "Refinement of a Design-Oriented Stress-Strain Model for FRP-Confined Concrete." ASCE J. Compos. Constr. 13(4): p. 269-278.

Wang, Z. Y., Wang, D. Y., Smith, S. T., and Lu, D. G. (2012). "CFRP-confined square RC columns. I: Experimental investigation." J. Compos. Constr., ASCE, 16(2), 150-160.

Wang, L. M., and Wu, Y. F. (2008). “Effect of Corner Radius on the Performance of CFRP-Confined Square Concrete Columns: Test.” Eng. Struct., 30(2): p. 493-505.

Wei, Y.Y., Wu, Y.F. (2012). “Unified stress–strain model of concrete for FRP-confined columns.” Constr Build Mater; 26(1): 381-92.

Wu Y.F., and Wei Y.Y. (2010). “Effect of cross-sectional aspect ratio on the strength of CFRP-confined rectangular concrete columns.” Eng Struct; 32: 32-45.

Yamakawa, T., Zhong, P., and Ohama, A. (2003). “Seismic Performance of Aramid Fiber Square Tubed Concrete Columns with Metallic and/or Non-metallic Reinforcement” Journal of Reinforced Plastics and Composites, 22, 13, pp 1221-1237.

Youssef, M.N., Feng, M. Q., and Mosallam, A. S. (2007). “Stress-strain model for concrete confined by FRP composites.” Composites Part B: Engineering, 38(5-6): p. 614-628.

Zaghi, A.E., Saiidi, M.S., and Mirmiran, A. (2012). “Shake table response and analysis of a concrete-filled FRP tube bridge column.” Composite Structures, 94 (5), 164-1574.

Table 1. Properties of test specimens

Specimen			FRP tube				
Designation	Description	Dimensions (mm)	Number of layers	Corner radius (mm)	Corner strengthening	Internal panel	Fiber sheet length (mm)
RL3	Reference	150x300x600	3	40	NA	N/A	2794
RL3CS1C	Corner Strengthened		3		1-layer CFRP strips		3245
RL3SC2C			3		2-layer CFRP strips		3697
RL4CS2C			4		2-layer CFRP strips		4628
RL3IP3C	Internal Panel		3		N/A	3-layer CFRP panel	3444
RL3RIP3C			3			3-layer rounded CFRP panel	3375
RL3IP6C			3			6-layer CFRP panel	4094
RL3IP6G			3			6-layer GFRP panel	CFRP:2994 GFRP:1500
RL3IP9G			3			9-layer GFRP Panel	CFRP:2994 GFRP:2250
SL5	Square CFFT made of cylinders	200x200x600	5	50	N/A	4 x 2-layer cylinders	5056

Table 2. Properties of fiber sheets and FRP composites

Type	t_f (mm/ply)	Fiber weight (g/m^2)	Manufacturer supplied fiber properties			Properties of FRP composites obtained from coupon tests		
			f_{fu} (MPa)	ε_{fu} (%)	E_f (GPa)	f_{fu} (MPa)	ε_{fu} (%)	E_f (GPa)
Carbon	0.117	200	3800	1.55	240	3422	1.38	248
Glass	0.154	400	2400	3.30*	73	2303	3.03	76

t_f = nominal fiber thickness, f_{fu} = tensile strength, ε_{fu} = ultimate tensile strain, E_f = elastic modulus

*Calculated from f_{fu} and E_f assuming linear elastic behaviour

Table 3. Failure locations of specimens

Specimen	Failure location
RL3	Corner region
RL3CS1C	Corner region
RL3SC2C	Span region along the long side of the cross-section
RL4CS2C	Span region along the long side of the cross-section
RL3IP3C	Span region along the long side of the cross-section near the internal panel connection. Also some damage on the internal panel
RL3RIP3C	Internal panel external tube connection
RL3IP6C	Span region along the long side of the cross-section near the internal panel connection. Internal panel intact
RL3IP6G	Span region along the long side of the cross-section near the internal panel connection. Internal panel intact
RL3IP9G	Corner region. Failure is affected by the load eccentricity experienced during the testing
SL5	Corner region. Internal cylinders also ruptured along regions that corresponded to the corners of the external tube

Table 4. Transverse strains recorded at failure

Specimen	Transverse Strains at Failure				
	Average ($\mu\varepsilon$)	Long-span ($\mu\varepsilon$)	Short-span ($\mu\varepsilon$)	Corner ($\mu\varepsilon$)	Near corner ($\mu\varepsilon$)
RL3	6346	4761	7805	5364	7453
RL3CS1C	8159	7511	10742	6715	7669
RL3SC2C	8294	8079	11342	5856	7902
RL4CS2C	8027	9789	10571	4505	7242
RL3IP3C	7834	10799	6128	5214	9197
RL3RIP3C	6462	7791	5659	4861	7540
RL3IP6C	8298	13873	6414	4957	7951
RL3IP6G	8888	13247	7099	6108	9099
RL3IP9G	7456	9235	6065	7070	7452
SL5	8869	8822*		8963	N/A

*Span average

Table 5. Test results

Specimen	f'_{ct} (MPa)	f'_{cc} (MPa)	ε_{cu} (%)	f'_{ct}/f'_{co}	f'_{cc}/f'_{ct}	f'_{cc}/f'_{co}	$\varepsilon_{cu}/\varepsilon_{co}$
RL3	24.4	23.8	1.38	0.91	0.98	0.89	6.3
RL3CS1C	25.8	26.7	1.94	0.97	1.03	1.00	8.8
RL3SC2C	26.2	30.1	2.11	0.98	1.15	1.13	9.6
RL4CS2C	27.5	35.3	3.07	1.03	1.28	1.32	14.0
RL3IP3C	26.2	33.0	1.81	0.98	1.26	1.24	8.2
RL3RIP3C	26.7	40.7	1.72	1.00	1.52	1.52	7.8
RL3IP6C	26.5	36.9	1.84	0.99	1.39	1.38	8.4
RL3IP6G	26.4	38.5	2.33	0.99	1.46	1.44	10.6
RL3IP9G	26.6	33.9*	1.85*	1.00	1.27*	1.27*	8.4*
SL5	33.3	83.0	3.58	1.25	2.49	3.11	16.3

* Specimen failed prematurely

Table 6. Relative performances of specimens

Specimen	S_{spec}/S_{ref}	$(f'_{cc})_{spec}/(f'_{cc})_{ref}$	$(\varepsilon_{cu})_{spec}/(\varepsilon_{cu})_{ref}$
RL3	1.00	1.00	1.00
RL3CS1C	1.16	1.12	1.41
RL3SC2C	1.32	1.26	1.53
RL4CS2C	1.66	1.48	2.22
RL3IP3C	1.23	1.39	1.31
RL3RIP3C	1.21	1.71	1.25
RL3IP6C	1.47	1.55	1.33
RL3IP6G	1.61	1.62	1.69
RL3IP9G	1.88	1.42	1.34
SL5	1.81	3.49	2.59

Table 7. Model predictions of ultimate condition of a circular CFFT analogous to Specimen SL5

Model	f'_{cc} (MPa)	ε_{cu} (%)	$(f'_{cc})_{model}/(f'_{cc})_{SL5}$	$(\varepsilon_{cu})_{model}/(\varepsilon_{cu})_{SL5}$
Bisby et al. (2005)	75.2	2.22	0.91	0.62
Teng et al. (2007)	72.1	2.49	0.87	0.70
Youssef et al. (2007)	74.5	3.05	0.90	0.85
Teng et al. (2009)	68.4	2.44	0.82	0.68
Wei and Wu (2012)	76.2	2.86	0.92	0.80

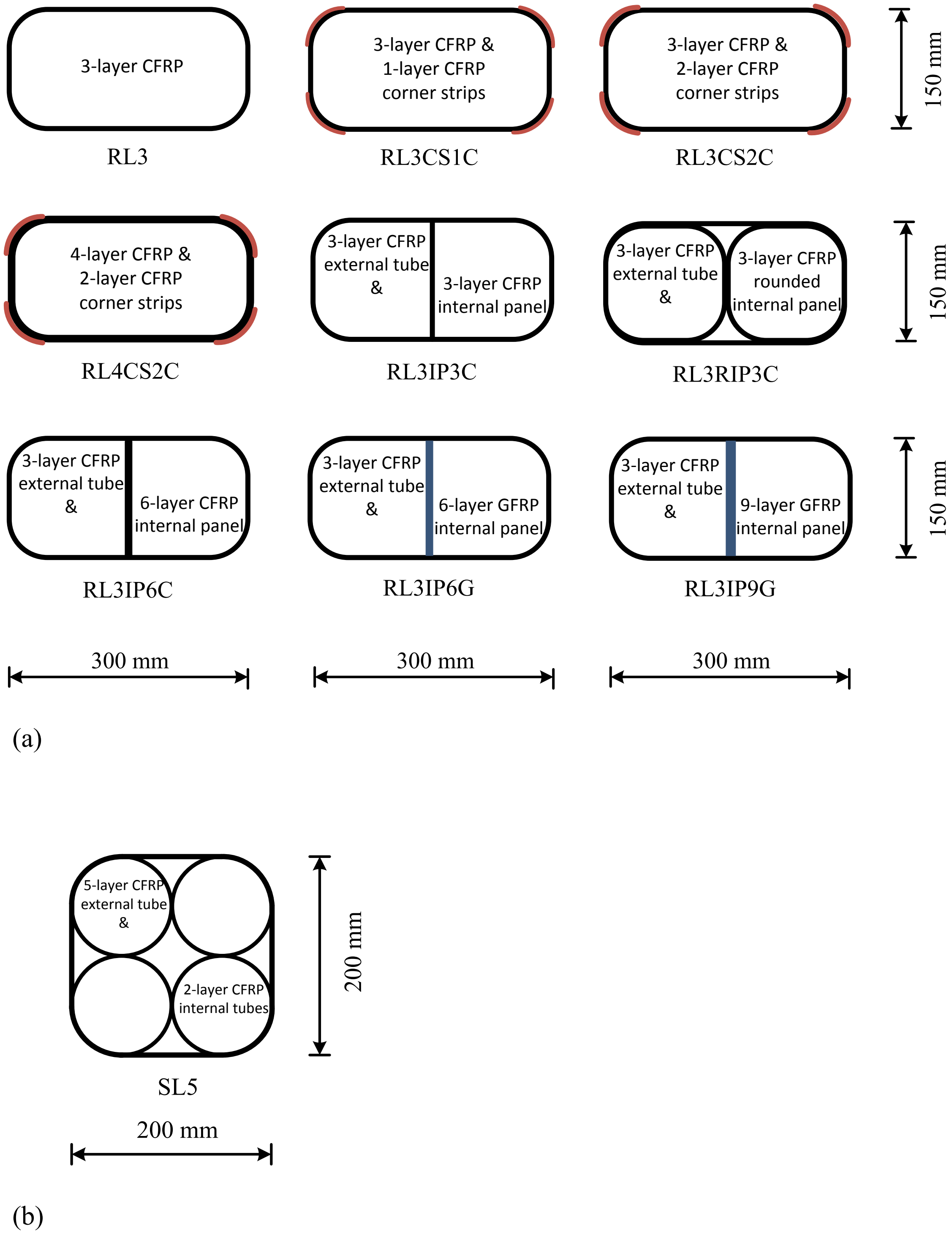

Figure1. Cross-sections of test specimens: (a) rectangular specimens; (b) square specimen

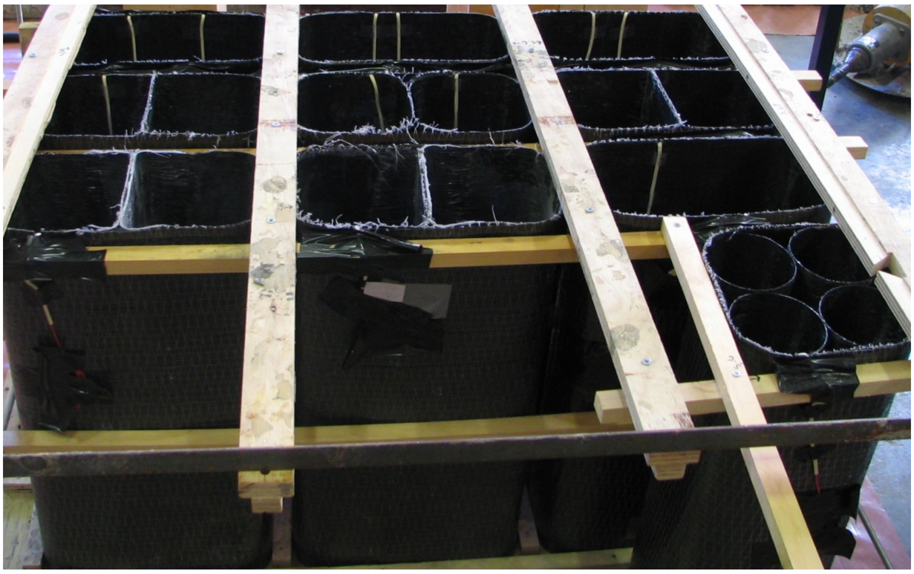

Figure 2. FRP tubes before casting of concrete

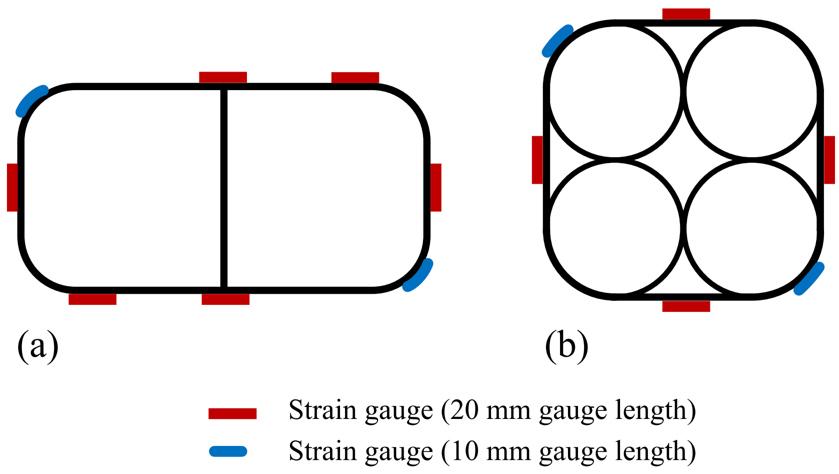

Figure 3. Locations of transverse strain gauges: (a) rectangular specimens; (b) square specimen

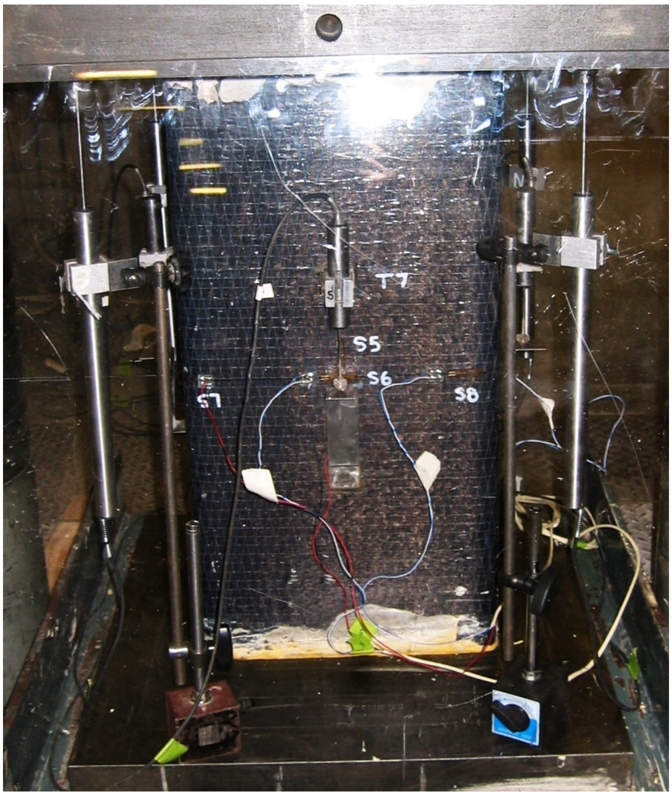

Figure 4. Test setup and instrumentation

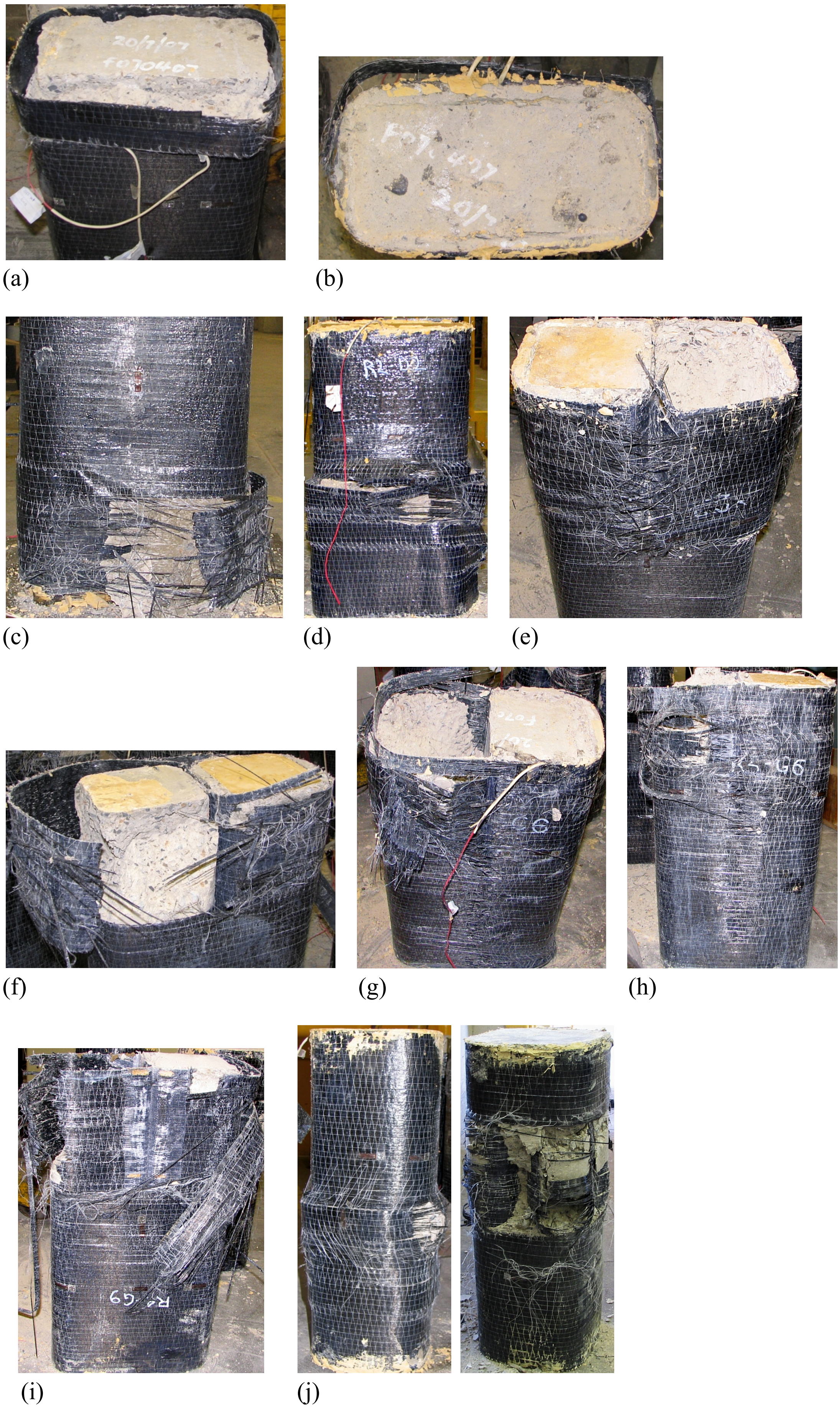

Figure 5. Failure modes of Specimens: (a) RL3; (b) RL3CR1; (c) RL3CR2; (d) RL4CR2; (e) RL3IP3C; (f) RL3RIP3C; (g) RL3IP6C; (h) RL3IP6G; (i) RL3IP9G; (j) SL5

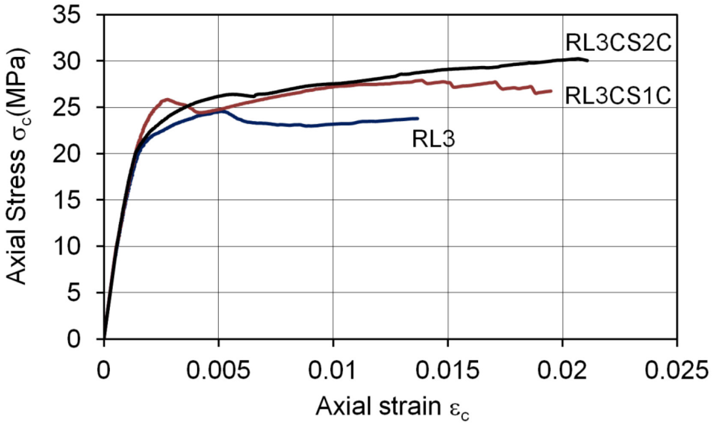

Figure 6. Stress-strain behavior of CFFTs with corner strengthening

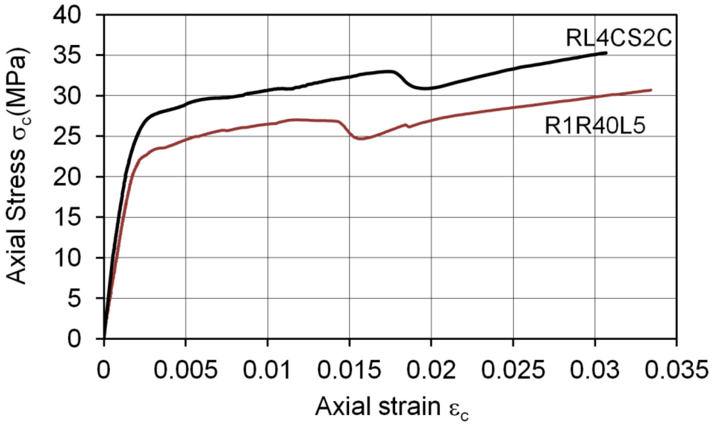

Figure 7. Corner strengthening versus addition of a full layer

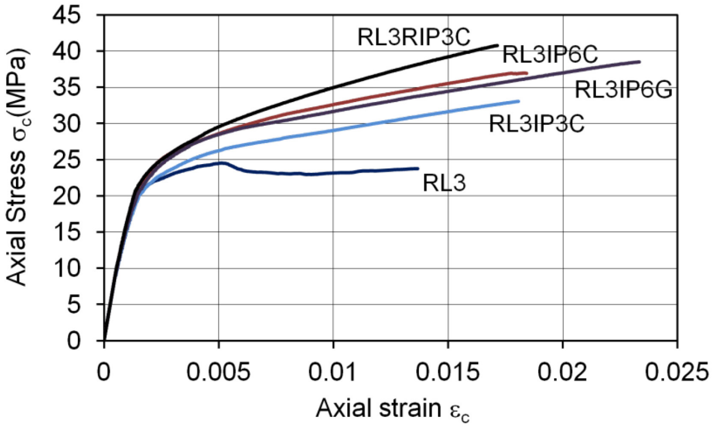

Figure 8. Stress-strain behavior of CFFTs with an internal panel

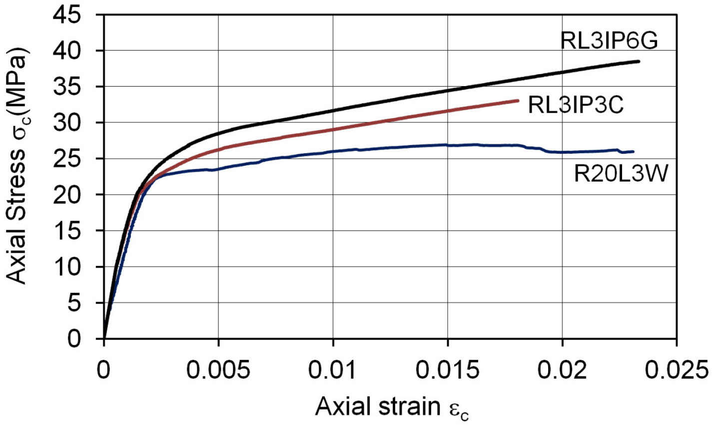

Figure 9. Influence of corner radius on axial compressive behavior of CFFTs with an internal panel

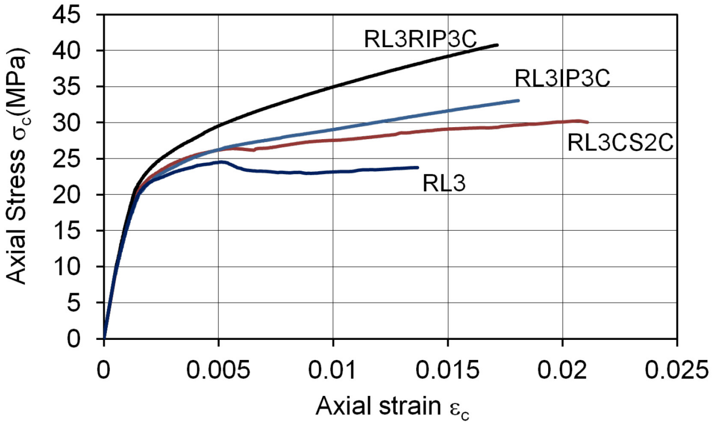

Figure 10. Comparison of stress-strain behaviors of CFFTs manufactured using different enhancement techniques

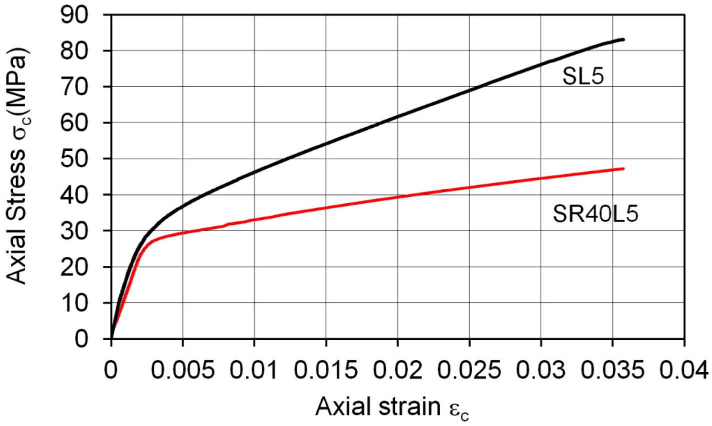

Figure 11. Stress-strain behavior of square CFFT made of concrete-filled FRP cylinders

List of Figures

List of Tables